J. Fluid Mech. (1988), *vol.* 193, *pp.* 217–241
Printed in Great Britain

On the viscous deformation of biological cells under anisotropic surface tension

By DANIEL ZINEMANAS AND AVINOAM NIR
Department of Chemical Engineering, Technion-Israel Institute of Technology, Haifa 32000, Israel

(Received 21 April 1987 and in revised form 16 October 1987)

A fluid-mechanical approach for the cleavage of biological cells is presented. The equations of motion were combined with concentration and orientation distribution balances, for active contractile filaments on the cell surface, to provide a dynamic evolution of interfacial forces and deformation. The resulting flow and the simultaneously developing surface-tension anisotropy provided a mechanism that facilitates the generation of a contractile ring at the cell equator: a major organelle in the establishment of cell furrow and the ultimate cleavage. The moving-boundary problem was solved numerically using boundary-integral representation for the Stokes equations which was modified to incorporate the anisotropic interfacial tensions.

1. Introduction

Cell deformation occurs in many biological systems and is caused either by the influence of the surrounding medium (e.g. blood flow) or by the cell's own activity (e.g. cell division). Modelling of such events usually uses a representation of the biological cells as viscous droplets (Greenspan 1977*a*, *b*; Gallez 1984) or microcapsules (Barthes-Biesel 1980), i.e. a viscous droplet surrounded by a thin membrane. These hydrodynamical descriptions of a cell differ mainly in the characteristics of the surface forces which may induce or oppose deformations.

A purely viscous-droplet description of a biological cell implies that the cell surface forces are modelled by surface tension typical of fluid–fluid interfaces. There, important processes known as capillary phenomena (Levich & Krylov 1969) may appear either when the interface shows a given curvature or when surface-tension gradients exist. The former effect gives rise to forces normal to the interface which are directly proportional to the magnitudes of the surface tension and the surface curvature. By opposing shape deformations, they have a stabilizing effect on the system. Gradients of surface tension, on the other hand, generate forces tangent to the interface. They derive from the surface-tension dependence on temperature or concentration of surface-active substances, which evidently alter the energy of the system. The effect of these tangential forces can be highly destabilizing.

In the case of the cell a surface-active substance corresponds to different biochemical species that are present at the cell surface and may thus alter its properties and behaviour by their chemical activity. Concentration gradients of such components may be controlled by mass transport from the inner or outer fluid as well as by reactions taking place at the interface.

Since the composition of the cell surface and its rheological properties are significantly different from the inner cytoplasm and the surrounding viscous

medium, it proves useful to represent a cell as an encapsulated viscous droplet whenever the surface remains homogeneous and does not exhibit active forces. Barthes-Biesel (1980) and Barthes-Biesel & Sgaier (1985), for example, simulated the behaviour of a spherical red blood cell in a shear flow using this approach. The rheological properties of the membrane were assumed to be linear elastic or linear viscoelastic.

An interesting example of cell deformation due to active surface forces is provided by cytokinesis, i.e. the late stage of cell division in which a cell divides physically into two new daughter cells. In this phenomenon the active organelle responsible for the cell cleavage is a thin layer just beneath the cell membrane, known as cortex, which is composed of a network of muscle-like contractile filaments. These filaments are observed to be oriented parallel to the cleavage plane under the leading furrow edge, forming an organelle known as the contractile ring which exerts the main driving force in the process (see reviews by Conrad & Rappaport 1981; Schroeder 1981*a*). The search for a better understanding of this phenomenon has led to the development of various theoretical models which were aimed at giving an explanation of the experimental data available and corroborating suggested mechanisms of cleavage. These models may be classified into two groups according to the hydrodynamical approach used to describe the surface forces.

One group consists of a solid-mechanics approach as exemplified by the works of Pujara & Lardner (1979) and Akkas (1980, 1981) and include forces of the membrane type. These authors modelled cytokinesis by studying the deformation of an initially spherical two-dimensional membrane that envelops a volume of fluid and which is subject to an equatorial constriction force. The membrane representing the overall surface layer was assumed to have isotropic nonlinear elastic or viscoelastic properties, while the effect of the viscous dissipation in the inner and outer regions was neglected. Membrane deformed shapes obtained agree satisfactorily with the cell deformations observed by Hiramoto (1968) regardless of the particular rheological model assumed. The model provides no insight into the dynamics of the process and the mechanism for the formation of the contractile ring.

Pure hydrodynamical models of cytokinesis were inspired by early experiments conducted by Butschli (1876) and Spek (1918) and their methodical reproduction by Greenspan (1978). These experiments show that a neutrally buoyant oil drop could undergo shape changes that closely resemble macroscopically the cell deformations during the cleavage process, when the drop surface tension at the poles is symmetrically lowered by means of an active surface substance. Based on these observations, Greenspan (1977*a*) suggested that hydrodynamical effects could play an important role in the cytokinetic process and give some insights into the mechanism that leads to the formation of a cleaving furrow and a contractile filamentous ring underneath. Greenspan (1977*a*, *b*) modelled the cell as a fluid droplet and the surface forces by an effective isotropic tension positively dependent on the concentration of contractile elements. Thus, if the droplet surface tension is lowered at the poles, owing to the effect of some stimulatory activity, a tension gradient produces a surface flow directed from the poles to the equator which causes an agglomeration of elements at the drop equator, further increasing the tension there and the overall surface-tension gradient. Greenspan postulated that this unstable process, once started, will continue indefinitely, providing the mechanism for cell cleavage. Moreover, it was suggested that in their motion toward the equator the contractile filaments rotate and reorient themselves parallel to the cleavage plane

owing to surface contraction. His asymptotic analysis describes the initial stages of shape deformation but is limited to small perturbations. A numerical calculation (Sapir & Nir 1985) for large deformations indicates that Greenspan's model, although providing a mechanism for the contractile ring formation, does not lead to complete cleavage owing to the isotropic nature of the surface tension (Sapir & Nir 1985; White & Borisy 1983).

Recently, a model emphasizing the importance of the anisotropic character of the cell surface, an idea originally suggested by White & Borisy (1983), successfully demonstrated the deformation and division of spherical cells (Zinemanas & Nir 1987). These results confirm that a better representation of the interfacial layer should be made to replace the effective surface tension or 'membrane' used in previous models.

In this communication we present a fluid-mechanical evaluation of the cytokinetic surface deformation ultimately leading to cell cleavage. The model combines the macroscopic equations of motion with microscopic local balances for filament concentration and orientation distribution function which are required to follow the local properties of the surface layer. The latter balances also involve a biochemical scheme representing the effects of surface stimulation and filament activity. Surface forces are evaluated as ensemble combinations of the individual contributions of the contractile elements. In §2 we outline the mathematical formulation for the moving-boundary problem. The slow viscous flow equations are combined with the material balances and the formulation of the interfacial forces into the form of a boundary-integral equation representation. This application to a problem with anisotropic interfacial forces is new. Simplifying assumptions are introduced in §3 to reduce the cumbersome equations to a form that is less complicated yet preserves the essentials of the full problem. The numerical scheme used is presented in §4 and the results are described in §5 where relevance to experimental observation is also discussed.

2. Biomechanical model

2.1. *Formulation of the flow problem*

Consider a droplet B of viscosity $\lambda\mu$, surrounded by a two-dimensional layer ∂B, freely suspended in an ambient infinite fluid B^* of viscosity μ. Both fluids are regarded as incompressible and Newtonian. This is a simplifying but rather well-justified assumption since, although it is known that the cytoplasm exhibits viscoelastic rheological properties (Hiramoto 1968), their role in the relatively slow process of cytokinesis is of secondary importance. Support for this conclusion is provided by the observations that substitution of a considerable part of the cytoplasm by oil or physiological solutions did not show any phenomenological or marked dynamic changes in cell cleavage (Hiramoto 1956). The Reynolds number of the flow is given by $\rho Ua/\mu$ where U is a representative velocity of the system, a the characteristic droplet dimension and ρ is the density of the fluid. When the driving force responsible for the motion and droplet deformation are the interfacial tensions of characteristic value, γ_0, and gradient, $|\nabla\gamma|_0$ the velocity U corresponds to the normal and tangential interfacial motions which are of order $\gamma_0/\mu(1+\lambda)$ and $a|\nabla\gamma|_0/\mu(1+\lambda)$, respectively. Estimates of the Reynolds number based on cell typical values indicate that it is generally much less than unity except when local surface gradients are extremely high.

In the absence of inertial and gravity effects, the velocity $\boldsymbol{v}$, the stress $\boldsymbol{\sigma}$, and the pressure P fields in B and B^* obey the linear quasi steady equations of motion

$$\nabla \cdot \boldsymbol{\sigma} = 0, \tag{2.1}$$

$$\nabla \cdot \boldsymbol{v} = 0, \tag{2.2}$$

where

$$\boldsymbol{\sigma} = -P\boldsymbol{I} + \lambda\mu(\nabla \boldsymbol{v} + \nabla \boldsymbol{v}^{\dagger}) \tag{2.3}$$

with μ replacing $\lambda\mu$ in B^*.

The complementary boundary conditions to be satisfied are

$$\boldsymbol{v} \to 0 \quad \text{as } |\boldsymbol{x}| \to \infty, \tag{2.4}$$

$$\left.\begin{aligned} \Delta \boldsymbol{v} &= 0 \\ \Delta(\boldsymbol{\sigma} \cdot \boldsymbol{n}) &= \boldsymbol{f} \end{aligned}\right\}, \quad \boldsymbol{x} \in \partial B. \tag{2.5, 2.6}$$

Here, Δ denotes a difference across the surface (outer minus inner), $\boldsymbol{f}$ is the interfacial force exerted on the fluids and $\boldsymbol{n}$ is a unit vector normal to ∂B, pointing into B^*. The specific expression for the interfacial forces is derived in the next section.

Finally, if the interface ∂B, is described in terms of the radius vector $\boldsymbol{R}(\boldsymbol{x}, t)$, its kinematics is given by the condition

$$\frac{\mathrm{d}\boldsymbol{R}}{\mathrm{d}t} = \boldsymbol{v}, \quad \boldsymbol{x} \in \partial B, \tag{2.7}$$

where $\mathrm{d}/\mathrm{d}t$ denotes a material derivative.

2.2. *Interfacial forces*

In view of the structure and composition of the interfacial layer it is necessary, when deriving an appropriate expression for the forces there, to assume a structural approach in which the individual contributions of the components forming this layer are taken into account. It will be assumed that the interfacial layer is composed of rod-like particles which are able to exert a contractile force along their axis and are confined to a continuous matrix, ∂B. This implies that the overall force $\boldsymbol{f}$ is a combination of an active contribution from the particle network and the passive reactions of the matrix. The former is dependent on the local particle concentration c and their orientation distribution function N. The latter, however, depends on the surface strain and rate of deformation, via the rheological properties of the surface matrix. Following Aris (1962), with surface coordinates u_α ($\alpha = 1, 2$), the general expression for the force $\boldsymbol{f}$ is given by

$$\boldsymbol{f} = \gamma^{\alpha\beta}|_{\beta} \boldsymbol{R}_{,\alpha} + b_{\alpha\beta}\gamma^{\alpha\beta}\boldsymbol{n}, \tag{2.8}$$

where $\gamma^{\alpha\beta}$ is the surface contravariant stress tension, $\boldsymbol{R}_{,\alpha}$ and $\boldsymbol{n}$ are the covariant base vectors and $b_{\alpha\beta}$ is the second fundamental form of the surface. A comma indicates common differentiation and the bar denotes covariant differentiation which, in terms of the Christoffel symbols $\Gamma^{\gamma}_{\alpha\beta}$, is defined by

$$\gamma^{\alpha\beta}|_{\beta} = \gamma^{\alpha\beta}{}_{,\beta} + \Gamma^{\alpha}_{\beta\delta}\gamma^{\beta\delta} + \Gamma^{\beta}_{\beta\delta}\gamma^{\alpha\delta}. \tag{2.9}$$

Likewise, as we have concluded before, the tension $\gamma^{\alpha\beta}$ is separated in this case into the active and passive parts

$$\gamma^{\alpha\beta} = \gamma^{\alpha\beta}_{(\mathrm{p})}(c, N) + \gamma^{\alpha\beta}_{(\mathrm{m})}(e_{\alpha\beta}, \dot{e}_{\alpha\beta}) \tag{2.10}$$

where $e_{\alpha\beta}$ and $\dot{e}_{\alpha\beta}$ are the covariant strain and rate of strain tensions, the indices (p) and (m) denote the particle network and the matrix respectively, and the dot

indicates a time differentiation. In this expression knowledge of the local and instantaneous concentration and orientation distribution of filaments is required. Since the particles are confined to ∂B the dynamic evolution of these variables obeys surface mass and orientation conservation balances. These balances can be easily obtained by means of the surface Reynolds transport theorem (Aris 1962; Waxman 1984). The mass balance is of the form

$$\frac{\partial c}{\partial t}+v^{\alpha}c|_{\alpha}=-c[v^{3}a^{\alpha\beta}b_{\alpha\beta}+v^{\alpha}|_{\alpha}]+D_{\mathrm{T}}a^{\alpha\beta}c|_{\alpha\beta}+\hat{R}, \tag{2.11}$$

where v^{α} and v^{3} are the contravariant components of the tangential and normal surface velocities, D_{T} is the translational diffusion coefficient, $\hat{R}$ is the rate of filament production by chemical reaction and $a^{\alpha\beta}$ is the contravariant surface metric tensor. In contrast to the three-dimensional mass balance, (2.11) has an additional term which takes into account the surface deformations.

In deriving the orientation balance it was assumed that filaments are rigid slender bodies. This balance may be influenced by translational and rotational surface motion, translational and rotational diffusion and by reaction effects. In terms of the orientation distribution function, $N(\boldsymbol{x}, \boldsymbol{p}, t)$, the following expression is obtained:

$$\frac{\partial N}{\partial t}+v^{\alpha}N|_{\alpha}=D_{\mathrm{R}}\nabla^{2}_{(\mathrm{p})}N+\boldsymbol{\nabla}_{(\mathrm{p})}\cdot(\boldsymbol{w}N)+\frac{\hat{R}}{c}(\hat{N}-N)+\frac{D_{\mathrm{T}}}{c}(c|^{\alpha}N|_{\alpha}). \tag{2.12}$$

Here, D_{R} is the rotational diffusion coefficient, $\boldsymbol{p}$ is the unit vector along the particle axis, $\hat{N}$ denotes the orientation distribution function of filaments produced at rate $\hat{R}$, $\boldsymbol{w}$ is the particle angular velocity and $\boldsymbol{\nabla}_{(\mathrm{p})}$ denotes an operator with respect to the filament direction. This two-dimensional equation is an extended version of Burgers equation (Leal & Hinch 1971) including additional convective, reactive and translational diffusion effects. Note that the general three-dimensional counterpart of (2.12) has the same form except that there α takes the values 1, 2 and 3 and $\boldsymbol{p}$ and $\boldsymbol{x}$ are not confined or limited solely to ∂B.

The first term on the right-hand side accounts for the rotational diffusion of the particles while the second represents the effect of their rotational motion. The effect of the production of filaments and translational diffusion is manifested in the last two terms. Evidently these will not contribute to the orientation balance either when the particles are produced with the same orientation distribution $\hat{N}=N$ or when the gradients of c and N are perpendicular.

Since the particles are considered short compared with the droplet dimension and may be assumed smaller than the typical scale of surface velocity gradient variations, the local velocity field on ∂B in the vicinity of a particle may be considered linear. The appropriate expression for the angular velocity of a particle, $\boldsymbol{w}(\boldsymbol{p})$, is

$$\boldsymbol{w}=\epsilon_{\gamma\alpha}p^{\gamma}p^{\beta}(v^{\alpha}|_{\beta}-a^{\alpha\delta}b_{\delta\beta}v^{3})\,\boldsymbol{n}+\omega(\boldsymbol{p}) \tag{2.13}$$

where $\epsilon_{\alpha\beta}$ is the permutation tensor and $\omega(\boldsymbol{p})$ is an additional angular velocity appearing from possible interactions between adjacent particles, suggested by Schroeder (1975).

The contravariant components of the interfacial velocity in (2.11)–(2.13) are obtained by the following expressions:

$$v^{\alpha}=a^{\alpha\beta}[(\boldsymbol{I}-\boldsymbol{nn})\cdot\boldsymbol{v}]\cdot\boldsymbol{R}_{,\beta} \tag{2.14}$$

$$v^{3}=[\boldsymbol{nn}\cdot\boldsymbol{v}]\cdot\boldsymbol{n} \tag{2.15}$$

Generally, it may be more convenient to express the tensorial equations in terms of the physical components of the tensors (index in brackets) instead of the covariant and contravariant components. This is attained, for example, for the interfacial velocity or stresses, through the definitions

$$v^{(\alpha)} \equiv \frac{v^{\alpha}}{(a^{\alpha\alpha})^{\frac{1}{2}}}, \quad \gamma^{(\alpha\beta)} \equiv \frac{\gamma^{\alpha\beta}}{(a^{\alpha\alpha}a^{\beta\beta})^{\frac{1}{2}}} \text{ (no summation).} \tag{2.16}$$

Finally, the functional relationship between the surface stress tensor and the concentration and orientation distribution is required. Assuming that the forces the particles exert are conservative, a general expression for a filamentous network contribution to the tensile stresses is (Lanir 1983)

$$\gamma^{\alpha\beta}_{(\mathrm{p})} = \int_{\boldsymbol{p}} c \frac{\partial W(\boldsymbol{p})}{\partial e_{\alpha\beta}} N(\boldsymbol{p})\, \mathrm{d}\boldsymbol{p} \tag{2.17}$$

where $W(\boldsymbol{p})$ is the filament strain-energy function. It is interesting to note that although this filament's contribution to the surface stresses may depend on surface deformations through filament length variation, it has the form of a surface tension with anisotropic properties: the particles behave as a surface-active substance with a positive tension-concentration dependence and can make the cortex behave similarly to a fluid interface. In our case surface motion will be induced by concentration gradients as well as orientation variations. As mentioned before, the passive matrix contribution, $\gamma^{\alpha\beta}_{(\mathrm{m})}$ to the surface stresses depends on $e_{\alpha\beta}$ and $\dot{e}_{\alpha\beta}$ and is functionally determined by the cortex rheological properties. The latter can follow linear or nonlinear constitutive equation for interfacial layers (Evans & Skalak 1979; Waxman 1981, 1984; Adin Mann 1984).

The relative importance of diffusion effects in (2.11) and (2.13) is anticipated to be negligible since diffusion coefficients of macromolecules on cellular surfaces are extremely small (Edidin 1977). In the simplified problem presented in §3 we shall therefore neglect these effects compared to the convective terms in the two respective equations.

2.3. *Integral boundary equation*

In summary, (2.1)–(2.17) provide the formulation for the problem of the deformation of a viscous drop under the effect of surface tractions of the kind discussed in §2.2. Although, in this case, the equations of motion are quasi-steady and linear, the entire problem exhibits an unsteady and highly nonlinear behaviour due to the strong coupling appearing in the boundary conditions between the mass and orientation balances and the equations of motion. Furthermore, the drop shape, at which the boundary condition must be satisfied, is not known *a priori* but follows dynamic changes which are described by the kinematic condition (2.7).

The equations of motion (2.1), (2.2) may also be expressed in an alternative integral form. This integral expression is, in fact, a representation of the solution to the Stokes equations which was derived by Ladyzhenskaya (1969) and is expressed in terms of the hydrodynamical single and double layer potentials. The derivation is based on the fundamental solutions of the Stokes equations and exploits their linearity. The main advantages of this boundary-integral representation reside in the incorporation of the equations of motion and the boundary conditions into a single integral expression which is expressed in terms of the surface velocity and stress distributions only. This is of major importance since the principal task of this work

is to study the behaviour and deformation of the interfacial layer and, in particular, the dynamics of the surface tensions.

Rallison & Acrivos (1978) used the integral-equation approach to study the deformation of a viscous drop in an extensional flow field. Using the jump condition of the double layer potential Rallison & Acrivos derived a boundary-integral equation for the interfacial velocity. Their analysis applies to a constant surface tension and an arbitrary viscosity ratio, thus extending the previous expressions obtained by Youngren & Acrivos (1975, 1976) for the particular cases of $\lambda \to \infty$ and $\lambda = 0$. A similar approach was used by Hiram & Nir (1983) to study the coalescence of two spherical polymer drops due to surface-tension forces, and by X. Z. Li, D. Barthes-Biesel & A. Helmy (1986, private communication) to determine the behaviour of a microcapsule in a shear flow. Likewise, the boundary-integral approach was found useful in evaluating the motion of a spherical particle normal to a deformable interface (Lee & Leal 1982; Geller, Lee & Leal 1986), and in the study of shear flows over two-dimensional ridges and cavities (Higdon 1985). Following Ladyzhenskaya (1969) and Rallison & Acrivos (1978), Sapir & Nir (1985) derived a similar expression for the interfacial velocity which also included a term involving the effects of surface-tension gradients on the surface forces.

The general integral equation for the interfacial velocity is of the form

$$\tfrac{1}{2}(1+\lambda)\,\boldsymbol{v}(\boldsymbol{x})+(1-\lambda)\int_{\partial B}\boldsymbol{K}(\xi):\boldsymbol{v}(\boldsymbol{y})\,\boldsymbol{n}(\boldsymbol{y})\,\mathrm{d}S_y=\boldsymbol{v}^{\infty}(\boldsymbol{x})-\frac{1}{8\pi\mu}\int_{\partial B}\boldsymbol{J}(\xi)\cdot\boldsymbol{f}(\boldsymbol{y})\,\mathrm{d}S_y,$$
$$\boldsymbol{x},\,\boldsymbol{y}\in\partial B, \quad (2.18)$$

where the kernels for the single and double layer potentials are, respectively,

$$\boldsymbol{J}(\xi)=\frac{\boldsymbol{I}}{\xi}+\frac{\xi\xi}{\xi^3}, \quad \boldsymbol{K}(\xi)=\frac{3}{4\pi}\frac{\xi\xi\xi}{\xi^5}, \quad \xi=\boldsymbol{x}-\boldsymbol{y}, \quad \xi=|\xi|. \tag{2.19}$$

Here $\boldsymbol{v}^{\infty}(\boldsymbol{x})$ denotes the imposed flow at $|x|\to\infty$ which must satisfy the creeping-flow equations. In our case $\boldsymbol{v}^{\infty}=0$. The most general form of the interfacial forces $\boldsymbol{f}$ is described by (2.8) and is related to the inner and outer fluid stresses by the condition (2.6).

Equation (2.18) is significantly simplified when $\lambda = 1$, attaining the explicit form

$$\boldsymbol{v}(\boldsymbol{x})=\boldsymbol{v}^{\infty}(\boldsymbol{x})-\frac{1}{8\pi\mu}\int_{\partial B}\boldsymbol{J}(\xi)\cdot\boldsymbol{f}(\boldsymbol{y})\,\mathrm{d}S_y. \tag{2.20}$$

Rallison & Acrivos (1978) noted that (2.20) is not limited to $\boldsymbol{x}$ in ∂B but is valid everywhere. This follows from the fact that when the same equation describes the motion of the inner and outer fluids, the velocity field is determined, owing to the linearity of the Stokes equations, by the imposed flow and the distribution of Stokelets which, in this case, corresponds to the interfacial forces $\boldsymbol{f}$. This argument is verified in (2.20) by noting that $\boldsymbol{J}(\xi)$ is the fundamental solution of the Stokes equation that denotes the velocity field at a point $\boldsymbol{x}$ due to a unit force exerted at $\boldsymbol{y}$.

Similarly, the integral expression for the pressure is given by (Ladyshenskaya 1969)

$$P(\boldsymbol{x})=-\int_{\partial B}\boldsymbol{L}(\xi)\cdot\boldsymbol{\sigma}(\boldsymbol{v}(\boldsymbol{y}))\cdot\boldsymbol{n}(\boldsymbol{y})\,\mathrm{d}S_y-\lambda\mu\int_{\partial B}\boldsymbol{M}(\xi):\boldsymbol{v}(\boldsymbol{y})\,\boldsymbol{n}(\boldsymbol{y})\,\mathrm{d}S_y, \quad \boldsymbol{x}\in B, \quad \boldsymbol{y}\in\partial B, \tag{2.21}$$

where

$$L(\xi) = -\frac{1}{4\pi}\frac{\xi}{\xi^3}, \quad \boldsymbol{M}(\xi) = -\frac{1}{2\pi}\left(\frac{\boldsymbol{I}}{\xi^3} - \frac{3\xi\xi}{\xi^5}\right). \tag{2.22}$$

For $\boldsymbol{x}$ in B^*, $\lambda\mu$ and $\boldsymbol{n}$ are replaced by μ and $-\boldsymbol{n}$, respectively.

The first integral is a single layer potential with density $\boldsymbol{n}$ which has a discontinuity of the first kind as $\boldsymbol{x}$ approaches ∂B (Ladyshenskaya 1969), with a jump equal to $\frac{1}{6}$ trace ($\boldsymbol{\sigma}$). For an incompressible fluid this jump becomes $\frac{1}{2}P$. Thus, noting that the second integral is continuous across ∂B, the values of the inner and outer pressures as $\boldsymbol{x}$ approaches ∂B from B and B^* are respectively

$$\tfrac{1}{2}P(\boldsymbol{x}^-) = -\int_{\partial B} L(\xi)\cdot\boldsymbol{\sigma}(\boldsymbol{v}(\boldsymbol{y}))\cdot\boldsymbol{n}(\boldsymbol{y})\,\mathrm{d}S_y - \lambda\mu\int_{\partial B}\boldsymbol{M}(\xi):\boldsymbol{v}(\boldsymbol{y})\,\boldsymbol{n}(\boldsymbol{y})\,\mathrm{d}S_y, \quad \boldsymbol{x}\in B, \tag{2.23}$$

$$\tfrac{1}{2}P(\boldsymbol{x}^+) = P^\infty(\boldsymbol{x}) + \int_{\partial B} L(\xi)\cdot\boldsymbol{\sigma}(\boldsymbol{v}(\boldsymbol{y}))\cdot\boldsymbol{n}(\boldsymbol{y})\,\mathrm{d}S_y + \mu\int_{\partial B}\boldsymbol{M}(\xi):\boldsymbol{v}(\boldsymbol{y})\,\boldsymbol{n}(\boldsymbol{y})\,\mathrm{d}S_y, \quad \boldsymbol{x}\in B^*. \tag{2.24}$$

Adding these expressions, a mean pressure may be defined at the interface:

$$P(\boldsymbol{x}) = \tfrac{1}{2}(P(\boldsymbol{x}^+)+P(\boldsymbol{x}^-)) = \int_{\partial B} L(\xi)\,\Delta\boldsymbol{\sigma}(\boldsymbol{y})\cdot\boldsymbol{n}(\boldsymbol{y})\,\mathrm{d}S_y + \mu(1-\lambda)\int_{\partial B}\boldsymbol{M}(\xi):\boldsymbol{v}(\boldsymbol{y})\,\boldsymbol{n}(\boldsymbol{y})\,\mathrm{d}S_y + P^\infty(\boldsymbol{x}), \quad \boldsymbol{x}\in\partial B \tag{2.25}$$

which, for $\lambda = 1$, simplifies to

$$P(\boldsymbol{x}) = P^\infty(\boldsymbol{x}) + \int_{\partial B} L(\xi)\cdot\boldsymbol{f}(\boldsymbol{y})\,\mathrm{d}S_y. \tag{2.26}$$

We shall make use of (2.20) and (2.26) in the evaluation of bulk properties as streamlines and pressures. As with (2.20), expression (2.26) is also valid for $\boldsymbol{x}$ in B and B^* since the pressure is determined by the imposed flow and the distribution of interfacial forces through the fundamental solution to the pressure field, L.

The continuity equation (2.2) may also be expressed in an integral form by applying the divergence theorem,

$$\int_{\partial B}\boldsymbol{v}\cdot\boldsymbol{n}\,\mathrm{d}S = 0. \tag{2.27}$$

This expression is used later to control the accuracy of the numerical evaluations and ensure that the solution indeed satisfies the incompressibility condition, i.e. the total volume of the drop remains constant.

3. A simplified model

3.1. *Assumptions*

In order to make the above system of equations solvable and at the same time maintain the basic phenomenological characteristics of the cytokinetic process, a number of simplifying assumptions are made. A discussion of these based on biophysical and biochemical considerations is given in §3.2.

(*a*) The ratio of viscosities, λ, is taken to be 1.

(*b*) Terms involving translational and rotational diffusion in (2.11) and (2.12) are neglected.

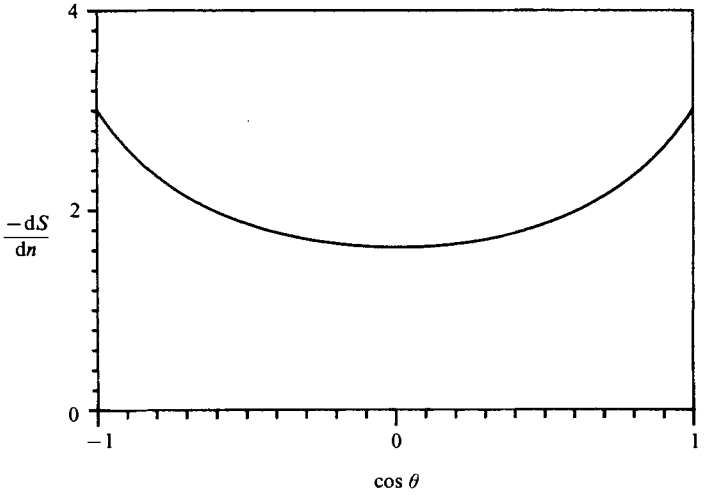

FIGURE 1. Stimulus flux at the initial spherical surface.

(*c*) Population distribution functions of passive and active filaments are equal and initially random.

(*d*) The rate of production of active particles at the surface is controlled, via a simple biochemical kinetic scheme, by a stimulating agent which diffuses to the surface from two source points located at the droplet axis. A plot of the stimulus flux at the initial spherical surface is shown in figure 1.

(*e*) Filaments exert a contractile force which is independent of their length but depends on time.

(*f*) Passive contributions to the surface stress, i.e. $\gamma^{\alpha\beta}_{(m)}$, are neglected.

(*g*) The interaction between adjacent filaments results in an additional rotation contributing to particle orientation.

3.2. *Discussion of the simplified model*

The assumptions in §3.1 are based on the following biophysical and biochemical considerations.

(*a*) The assumption that the ratio of viscosities λ, is 1 may not exactly reflect the biological situations, yet it greatly simplifies the integral boundary equation for the interfacial velocity but, on the other hand, does not have a significant qualitative influence on the drop surface dynamics (Hiram & Nir 1983). The deformation timescales, however, may differ.

(*b*) The equations of mass and orientation balances may be reduced since it is found that the coefficients for macromolecular translational and rotational diffusion on cell surfaces are extremely small (Edidin 1977). This argument is supported by the fact that the estimated length of the contractile filaments is 0.5 μm, close to the limit where Brownian motion effects become negligible. Mathematically, the typical Péclet number, defined by the characteristic values of the surface velocity, the filament length and the appropriate diffusion coefficient, is found to be high in all cytokinetic processes.

(*c*) Considering the hypothesis that active filaments are produced from passive filaments, by a biochemical reaction, and that both populations are initially

randomly oriented, it is expected that their orientation distribution functions are equal. This implies that the reactive terms in (2.12) can also be negligible.

In view of (*a*), (*b*) and (*c*), the equations of motion (2.1) and (2.2) can be described in the reduced integral form by (2.20) and (2.26), while the mass and orientation balances become

$$\frac{\mathrm{d}c}{\mathrm{d}t} = -c[v^3 a^{\alpha\beta} b_{\alpha\beta} + v^{\alpha}|_{\alpha}] + \hat{R} \tag{3.1}$$

and

$$\frac{\mathrm{d}N}{\mathrm{d}t} = \nabla_{(\mathrm{p})} \cdot (\boldsymbol{w} N). \tag{3.2}$$

The initial conditions for (3.1) and (3.2) are that filaments are uniformly distributed and randomly oriented in the cortical sublayer. This conforms with the evidence that the cell cortex does not exhibit any region particularly predisposed to form a contractile ring (Rappaport & Ebstein 1965) and that the interfacial tension is initially homogeneous and isotropic (Hiramoto 1968).

(*d*) The biochemical process from which the rate of production of filaments is estimated was assumed to follow the simple first-order kinetic scheme

$$\left.\begin{aligned} \mathrm{F} + \mathrm{E} &\overset{k_1}{\rightarrow} \mathrm{FE} \overset{k_2}{\rightarrow} \mathrm{A} \\ \mathrm{S} + \mathrm{E} &\overset{k_3}{\rightarrow} \mathrm{SE} \overset{k_4}{\rightarrow} \mathrm{B} \end{aligned}\right\} \tag{3.3}$$

here, F and FE denote the passive and active forms of the contractile filaments, S is a stimulatory biochemical agent sent by the mitotic apparatus to the cortex, and E is an activating agent. SE represents an inhibited form of E, and A and B constitute inactive byproducts of the above sequential process. The species F, E and FE are confined to the cortical layer.

In the absence of a complete known biochemical process, this scheme accounts for the major observed and expected phenomenological behaviours. These include, as the first reaction shows, a mechanism of filament activation that does not depend on the presence of a mitotic apparatus. This kind of activity was found in enucleated cells and is manifested by periodic variations in surface tension (Schroeder 1981*b*). The second characteristic included is a relaxation of the surface tension owing to the inhibition of the activity agent E by a stimulating agent. This is in agreement with the polar relaxation theory of cleavage which postulates that the stimulus produces a relaxation of the cortical tensions due to inhibition or decomposition of contractile filaments.

The biochemical stimulus is assumed to diffuse toward the surface from two point sources located at the asters of the mitotic apparatus in a finite time period during which the diffusion process is regarded stationary. The stimulatory agent S is considered to react relatively fast as it reaches the cortex. In this case the equation controlling the distribution of the stimulus is given by the Laplace equation

$$\nabla^2 S = 0, \quad \boldsymbol{x} \in B, \tag{3.4}$$

and is subject to the boundary conditions

$$S = 0, \quad \boldsymbol{x} \in \partial B \tag{3.5}$$

and a source of unit strength, located at each aster.

The solution to (3.4) for the flux on a spherical surface of radius unity and a distance of $2b$ between the astral sources, is given by

$$-\frac{\partial S}{\partial n}=\frac{1-b\cos\theta}{[1+b^2-2b\cos\theta]^{\frac{3}{2}}}+\frac{1+b\cos\theta}{[1+b^2+2b\cos\theta]^{\frac{3}{2}}}+\sum_{m=1}^{\infty} mA_m P_m(\cos\theta), \tag{3.6}$$

where θ is a meridional angle and P_m are Legendre polynomials with associated coefficients A_m. The total amount of the stimulus that reacts on the cortex then is calculated from the flux (3.6) and the time interval during which the sources are active. In figure 1 it can be seen that the highest level of influence is attained at the polar regions and therefore produces the strongest cortical tension relaxation there. In the numerical calculation the initial concentration of F, E and FE were chosen as 1, 2 and 0.5 respectively and the kinetic constants were selected to be $k_1 = 1$, $k_2 = 0.1$, $k_3 \to \infty$, $k_4 = 0$.

(*e*) Since the biochemistry behind muscle contractions is highly complex, involving a high number of steps and biochemical species (Goody & Holmes 1983), it is also assumed that each filament exerts the same contractile force K along its symmetry axis. In search of simplification it is considered that this force does not depend on the filament length, dl. Possible time variations in the filament forces are, however, permitted. To qualitatively retain the contraction–relaxation characteristics of isometric sarcomere tension dynamics of muscle activity, the filament force K was varied according to first-order kinetics,

$$\frac{\mathrm{d}K}{\mathrm{d}t}=\left(\frac{c_1}{1+c_1 t}-c_2\right)K. \tag{3.7}$$

c_1 and c_2 are arbitrary constants chosen merely to follow the process timescale.

(*f*) The passive contribution to the surface stress $\gamma^{\alpha\beta}_{(\mathrm{m})}$ arising from the cortical resistance to surface deformations is neglected here in the first approximation since most emphasis is given to the study of the behaviour and stresses of the filaments network. Inclusion of these forces does not enhance greatly the complexity of the equations and their solutions, while requiring the addition of several extra parameters into the model.

(*g*) The interaction between adjacent filaments, suggested by Schroeder (1975) induces an additional rotational motion which contributes to the filaments orientation. This effect is expressed in the second term on the right-hand side of (2.13). Since the mechanism of filament interaction is not known, a simple moment is assumed to exist between two filaments, allowing an analytical solution to the orientation balance (2.12).

The net moment $T(\alpha, \alpha')$ between a pair of particles at orientations α and α' results from attractive and retarding forces which originate from particle chemical composition, viscous resistance and steric hindrance, all not completely understood. This moment and the additional rotation it induces are expected to vanish when particles are either perpendicular or parallel in close proximity. For simplicity we assume that this characteristic has the explicit relation

$$T(\alpha, \alpha') \propto \sin 2(\alpha-\alpha'). \tag{3.8}$$

Superimposing the individual pair interactions of the particle at angle α with all particles at angles α' at a given position yields the additional rotation

$$\omega(\alpha)=\int_0^{\frac{1}{2}\pi} \beta N(\alpha') T(\alpha, \alpha')\,\mathrm{d}\alpha'. \tag{3.9}$$

Since the concentration of particles enhances the attractive components of the moment but also increases the viscous and steric retardation, the proportionality coefficient β is taken to be independent of c.

Evaluation of N from (3.2) following (3.9) will require cumbersome numerical iterations due to the nonlinear dependence. We therefore bring all interactions to the single orientation $\alpha' = \alpha_0$ with an intensity and direction dependent on the integrated tensions at each meridional location which is a macroscopic expression of the level of order there. α_0 is the orientation at which N attains its maximum.

Hence, we write

$$\omega(\alpha) = \int_0^{\frac{1}{2}\pi} \beta \left| \frac{4}{\pi} tg^{-1}\left(\frac{\gamma_{zz}}{\gamma_{\phi\phi}}\right) - 1 \right| \delta(\alpha' - \alpha_0) \sin 2(\alpha - \alpha') \, d\alpha'. \tag{3.10}$$

This permits a simple integration of (3.2) when $\alpha_0 = 0$ or $\frac{1}{2}\pi$.

3.3. *Axisymmetrical cleavage*

Although special cases of unilateral cleavages are encountered in nature or cleavages of experimentally altered cells have been obtained, the most common type of division is axisymmetrical, showing fore-and-aft symmetry. Thus, it is convenient to use a cylindrical coordinate system (r, ϕ, z) to describe the three-dimensional motions and a set of surface coordinates (ϕ, z) to follow the dynamics of the surface variables. These surface coordinates represent an orthogonal set which coincides with the principal axis of surface stresses, deformation, etc. The cell shape is defined by the even function $r = R(z)$ for $-l < z < l$.

The equations are non-dimensionalized using the scales γ_0, a and γ_0/μ for the surface tension, the distances and the velocities, respectively. Similarly, the pressure is normalized by $\gamma_0/a \cdot \gamma_0$ denotes a characteristic isotropic surface tension which, in view of (2.17), is proportional to the initial filaments concentration C_0. The latter was arbitrarily non-dimensionalized to be $\frac{1}{2}$.

Considering the axial symmetry of the motion, (2.20) can be integrated in the circumferential direction giving the simplified expression

$$\begin{bmatrix} v_r(z) \\ v_z(z) \end{bmatrix} = \int_{-l}^{l} \begin{bmatrix} A_{rr}(z-y) & A_{rr}(z-y) \\ A_{rr}(z-y) & A_{zz}(z-y) \end{bmatrix} \begin{bmatrix} f_r(y) \\ f_z(y) \end{bmatrix} dy, \tag{3.11}$$

where z and y are coordinates measured along the z-axis and $A_{rr}, A_{rz}, A_{zr}, A_{zz}$ are kernel functions, related to the tensor $\boldsymbol{J}$ derived by Youngren & Acrivos (1975) in terms of complete elliptic integrals (see Appendix A). f_r, f_z denote the cylindrical components of the interfacial forces which, when expressed in terms of the normal and tangential force components f_n and f_s, are

$$f_r = f_n n_r + f_s t_r, \quad f_z = f_n n_z + f_s t_z. \tag{3.12}$$

Here, $\boldsymbol{t}$ denotes a unit vector tangent to ∂B with components given by

$$t_r = -n_z = \frac{R'(y)}{[1 + R'^2(y)]^{\frac{1}{2}}}, \quad t_z = n_r = \frac{1}{[1 + R'^2(y)]^{\frac{1}{2}}}, \tag{3.13}$$

while it follows from (2.8) that f_n and f_s are related to the surface stress tensor, with principal values γ_{zz} and $\gamma_{\phi\phi}$, in the following manner:

$$f_n = \frac{\gamma_{zz}}{R_z} + \frac{\gamma_{\phi\phi}}{R_\phi}, \tag{3.14}$$

$$f_s = \frac{1}{[1+R'^2(y)]^{\frac{1}{2}}}\left[\frac{\partial \gamma_{zz}}{\partial y} + \frac{(\gamma_{zz}-\gamma_{\phi\phi})}{R(y)}\frac{\partial R}{\partial y}\right], \tag{3.15}$$

where the principal radii of curvature R_z, R_ϕ are given by

$$\frac{1}{R_z} = -\frac{R''(y)}{[1+R'^2(y)]^{\frac{3}{2}}}, \quad \frac{1}{R_\phi} = \frac{1}{R(y)[1+R'^2(y)]^{\frac{1}{2}}}. \tag{3.16}$$

The expression for the pressure (2.26) in this axisymmetrical case, with $P^\infty(\boldsymbol{x}) = 0$, is

$$P(r, z) = \int_{-l}^{l} [P_r(r, z, y) f_r(y) + P_z(r, z, y) f_z(y)]\, dy, \tag{3.17}$$

where P_r, P_z, the kernel functions related to the vector $\boldsymbol{L}$, are given in Appendix B.

In view of the simplifying assumptions the corresponding mass balance (2.11) takes the form

$$\frac{dc}{dt} = -c\left[v_n \nabla \cdot \boldsymbol{n} + \frac{1}{R(z)[1+R'^2(z)]^{\frac{1}{2}}}\frac{\partial (v_s R)}{\partial z}\right] + \hat{R}, \tag{3.18}$$

where v_n and v_s denote the normal and meridional-tangential velocity components. Using (2.14)–(2.16), or by simple geometry evaluations, these components are found to be related to the cylindrical velocity components through expressions similar to (3.12).

Similarly, designating the angle formed between the filament direction and a meridional line by α, the simplified version of the orientation balance (2.12) becomes

$$\frac{dN}{dt} = \frac{\partial}{\partial \alpha}(w(\alpha) N), \tag{3.19}$$

where, from (2.13), the angular motion reduces to

$$w = -\tfrac{1}{2}\sin 2\alpha\left[\frac{1}{[1+R'^2(z)]^{\frac{1}{2}}}\frac{\partial v_s}{\partial z} - \frac{v_s}{R(z)[1+R'^2(z)]^{\frac{1}{2}}}\frac{\partial R}{\partial z} + \left(\frac{1}{R_z} - \frac{1}{R_\phi}\right) v_n\right] + \omega. \tag{3.20}$$

As stated previously, the additional rotation ω results from the interaction between adjacent filaments.

Equation (3.19) subject to a randomly oriented initial filament distribution has a general solution of the form

$$N(\alpha, z, t) = \frac{1}{\cos^2\alpha \exp\left[-\int_0^t (w' + \Omega)\, dt\right] + \sin^2\alpha \exp\left[\int_0^t (w' + \Omega)\, dt\right]}, \tag{3.21}$$

where w' is the expression in the brackets on the right-hand side of (3.20). Here Ω denotes a constant of proportionality obtained by substituting (3.10) in (3.20).

Equation (3.21) provides the dynamic variations of the orientation distribution

function at any material point on the surface. In this expression, the integrals must be calculated numerically since the integrands are themselves dependent on the orientation distribution time history.

The dependence of surface stresses on the filament concentration and orientations is given in (2.17). Assuming, as stated previously, that each filament exerts a force K independent of its length, and that this length may be considered constant, the expression for the principal stresses of the filamentous network contribution is, in non-dimensionalized form,

$$\begin{bmatrix}\gamma_{zz}\\ \gamma_{\phi\phi}\end{bmatrix} = c(z,t)\int_0^{\frac{1}{2}\pi} N(\alpha,z,t)\begin{bmatrix}\cos\alpha\\ \sin\alpha\end{bmatrix}\mathrm{d}\alpha, \tag{3.22}$$

where the non-dimensional parameter $KdlC_0/\gamma_0$ is set to 1.

4. Numerical scheme

The nonlinearity and the coupling of the equations require the use of a numerical method for the solution of the above simplified problem. The quasi-steady nature of the equations of motion allows a simpler calculation scheme since the surface velocity may be determined from the known instantaneous shape and interfacial forces. This velocity may be employed in the mass and orientation balances and in the kinematic condition to evaluate, by means of an up-dated Lagrangian procedure, new concentration, orientation and tension profiles as well as a new shape. These are revised in a new calculation of surface velocities under the new conditions and thus the calculation scheme may be continued for as long as required.

The spatial derivatives and the velocity resulting from the integral (2.20) were evaluated using a finite-difference scheme. The contour of the axisymmetric surface was divided into M intervals by distributing $M+1$ points along a meridian line. Initially, these intervals were selected equal; however, any other arbitrary choice could have been used to anticipate crowding or separation of the material points under the effects of the surface motions and deformations. Since separation distances change as the points move, a finite-difference scheme for unequal intervals was employed while second-order accuracy was maintained when evaluating first and second derivatives using three- and five-point algorithms.

In evaluating surface velocities it is noted that as $\epsilon = z-y$ approaches zero, the kernel functions A in (3.11) possess a logarithmic singularity, except at the poles where this singularity is of $O(\epsilon^{-\frac{1}{2}})$, and therefore the expression is integrable everywhere. Thus, to evaluate the velocity at a given point x_n, the leading orders of the singular kernels, up to $O(\epsilon^2)$, were subtracted from the integrand in the interval between x_{n-1} and x_{n+1}. The regular integration which resulted was calculated using a trapezoidal rule and added to the analytical integration of the asymptotic singular expansion between x_{n-1} and x_{n+1}. Similar procedures were employed by Rallison & Acrivos (1978) and Hiram & Nir (1983).

$M = 70$ was used as a compromise between numerical accuracy and limited computer resources. A comparison of the results obtained by this algorithm to the analytical solutions for the surface velocities on a spherical drop having a constant or variable surface tension (Cox 1969; Sapir 1984) shows a close agreement to within a few percent.

Once the interfacial velocity was found, shape and orientation changes were

computed for each material point on the surface by means of a straightforward Newtonian integration which, for the shape variations, becomes

$$\boldsymbol{R}(t+\mathrm{d}t) = \boldsymbol{R}(t) + \boldsymbol{v}(t)\,\Delta t. \tag{4.1}$$

Since there is no obvious criterion for the stability of this quasi-steady evolution of the shape, an arbitrarily time increment Δt was chosen having the general form

$$\Delta t = C\frac{\mathrm{MIN}\,|\Delta \boldsymbol{x}|}{\mathrm{MAX}\,|\Delta \boldsymbol{v}|}, \tag{4.2}$$

where C is an $O(1)$ constant and $\boldsymbol{x}$ and $\boldsymbol{v}$ are the distance and velocity differences between any two adjacent points. This expression allows the sequential order of the points to be maintained and provides satisfactory numerical accuracy. The same increments were used in integration of the mass and orientation balances. For the mass balance, for example, the total cumulative errors were ever higher than 10% with the higher errors appearing during the very last stages of cleavage where extreme surface curvatures prevail.

The condition of incompressibility was maintained by correcting the normal velocity at each time-step by a small constant value to keep the drop value constant. This procedure is enforced since only integral estimates rather than local values of the normal velocity can be evaluated from the continuity equation (2.27). Typical corrections were $O(10^{-3})$ of the average surface normal velocity. If not corrected, the total volume increment would not exceed a few percent of the initial volume.

5. Results and discussion

Using the above numerical scheme, the mathematical model of cell cleavage presented in §3 was solved to analyse the role played by hydrodynamic motions in cell division and, particularly, in the reorganization of the cortical layer and the forces arising there.

As already stated, the initial biochemically uniform surface layer is altered by the flux of a stimulus from the mitotic asters towards the surface. According to (3.6) the effect of the flux is assumed proportional to its value and to the period of time during which the sources are active. This non-dimensional time interval was arbitrarily taken equal to 0.6 so that stimulus, sufficient to induce complete cleavage, can reach the surface. When shorter time intervals were used, cleavages were not fully accomplished since surface differentiation due to the stimulating action is not sufficient to later create the required surface organization and tension variations that would result in complete divisions. This is in agreement with the observation that when the mitotic apparatus is disrupted or eliminated at the earlier stages of mitosis, cleavage is inhibited or incompletely realized (Beams & Evans 1940; Hiramoto 1956).

The stimulating kinetic scheme results in a surface concentration profile of active contractile filaments that exhibits a concentration at the equator higher than at the poles. This developing concentration gradient, then, produces a surface-tension gradient which consequently induces a surface motion from the poles toward the equator. The surface flow thus created is responsible for the motion of filaments toward the equator as well as for part of the filament rotation as equations (3.18) and (3.19) indicate. A meridional tangential velocity profile typical of initial and

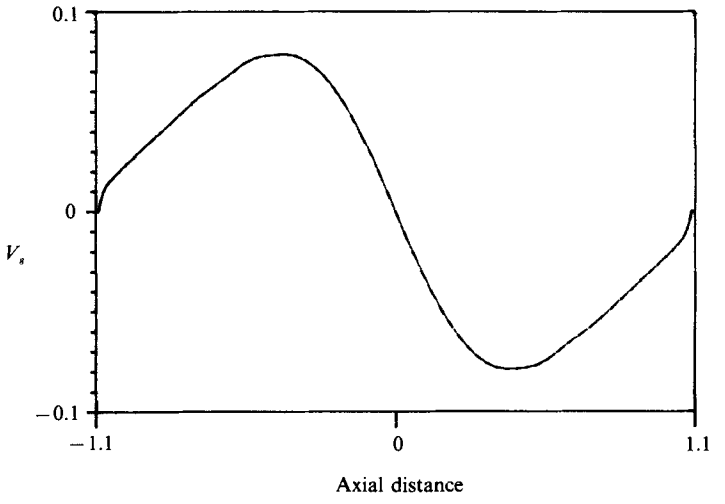

FIGURE 2. Tangential velocity profile at $t = 2$.

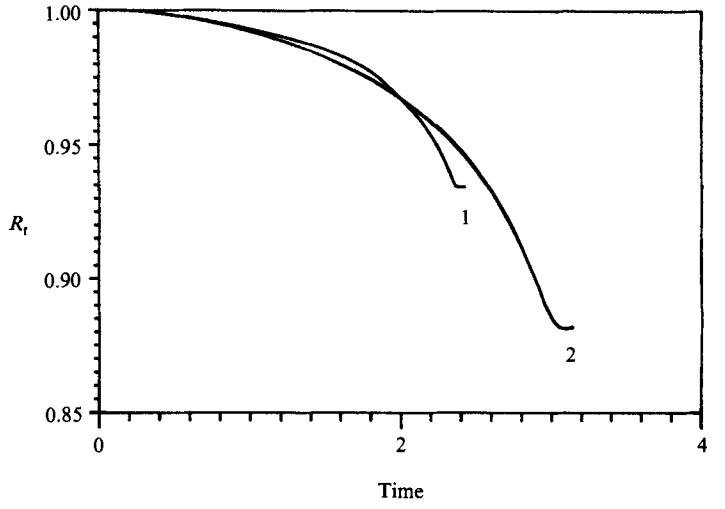

FIGURE 3. Furrow radius dynamics: a comparison between isotropic (1) and anisotropic (2) tension cases with no filament interactions and muscle dynamics.

intermediates times is shown in figure 2. This profile exhibits a region, around the equator, where the velocity gradient is negative, and two zones near the poles where this gradient is positive. Following (3.20), since the surface extensional flow field in which the filaments are confined decelerates near the equator, their rotational motion orients them there parallel to the cleavage plane. Note that since the initial orientation is random and that $R_z = R_\phi$ and $v_s = \partial R/\partial z = 0$ at the equator, the unique contribution to the rotational motions there is initially provided by the velocity gradient. This initial rotation then triggers the interaction between the filaments as the random orientation is disrupted. As the filaments rotate a gradient in the orientation distribution function is created. Its influence on the surface-tension gradient, particularly the meridional component, may be in the opposite direction to the influence of the already existing concentration profile.

We first discuss the influence of the orientation of filaments due to the sole effect of surface motions, i.e. neglecting the interaction effects and assuming no variations in the filaments force. The results are presented in figure 3 in terms of the dynamic changes of the furrow radius R_f, and are compared to the changes emerging in the isotropic-surface-tension case. In both situations cleavage is incomplete and the furrow radius shows a maximum reduction of about 10% of its initial value. Similar findings were reported for the isotropic-tension cases, by Greenspan (1977*a*, *b*) and by Sapir & Nir (1985) who could not achieve furrow reductions higher than 20% in spite of the various destabilizing surface force distribution they employed. Their conclusion was that isotropic surface tension could not lead to full cleavage owing to the high negative curvature that develops at the furrow leading edge. White & Borisy (1983) also failed to obtain complete cell cleavage whenever surface tensions were considered isotropic. They suggested the important role of anisotropic tensions in attaining complete divisions; however, they did not present their model rigorously.

The effect of the anisotropy in surface tension, due to the filaments reorientation, is seen in figure 3 to cause a further reduction of the furrow radius. This difference stems from the reorientation of the filaments in the equatorial region parallel to the cleavage plane which consequently increases the circumferential over the meridional tension. The resulting effect is a reduction of the influence of the meridional forces at the site of the developing negative radius of curvature R_z. However, the destabilizing effect of reorientation is not sufficient to completely overcome the negative curvature inhibiting factor, when caused by surface motions only, and being about a complete division. It is observed that while the furrow velocity in the initial stages of furrowing is higher in the anisotropic-surface-tension case this situation is later reversed. This behaviour may be explained in terms of the characteristic motion and reorientation particular to each case. Since at the beginning the filaments are oriented randomly, both situations exhibit similar concentration profiles and therefore their hydrodynamic behaviour is alike. As surface motion is induced and reorientation begins, a higher driving force is attained in the anisotropic case owing to the previously discussed enhancement of circumferential tension while the concentrations profiles in both cases remain similar. Later, as reorientation continues to increase the circumferential tension at the equator, the meridional tension component and its gradient diminish. Consequently, the surface motion responsible for the agglomeration of filaments in the equator decreases. Such an effect does not occur in the isotropic-tension case and the higher concentration achieved there results in higher furrow velocities. Maximum deflection is however smaller. It may be concluded, then, that the effect of the gradient of orientation distribution on the surface tension in the anisotropic-tension case opposes the effect of the concentration gradients.

When filaments interaction and muscle dynamics are included, division is achieved since, in this case, the degree of orientation at the furrow edge produces a differentiation between the circumferential and meridional equatorial tensions which is able to overcome the retarding effect of the negative principal curvature R_z. The influence of muscle dynamics of the form (3.7) is manifested in the modulation of the furrow velocity as is shown in figure 4. Since the force first increases and then gradually diminishes, the velocity at early stages appears higher than that evaluated when only interactions are included, but at later stages becomes smaller. This behaviour is in qualitative agreement with the measurements of Hiramoto (1968) and probably indicates that the force modulation and biochemical reactions denote important active processes in cell cleavage.

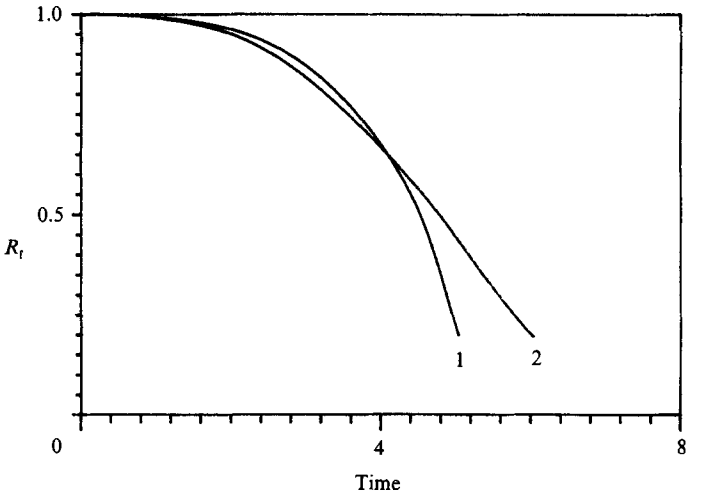

FIGURE 4. Furrow radius dynamics: (1) with filament interaction; (2) with filament interaction and muscle dynamics.

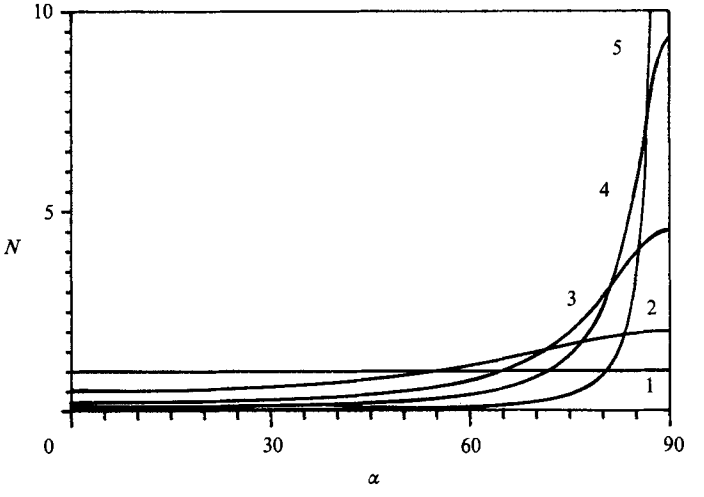

FIGURE 5. The evolution of orientation distribution functions at the equator: (1) $t = 0$, (2) 2, (3) 2.5, (4) 3, (5) 3.5.

The orientation distribution function related to the case in which interactions and muscle dynamics were included was evaluated in the equatorial region at several times and is presented in figure 5. In this region the filaments become oriented parallel to the cleaving plane owing to the effect of the negative tangential velocity gradient $\partial v_s/\partial s$ there, and the interaction between filaments according to (3.20). It is observed that sharp circumferential order is obtained after a relatively short period. In addition, the corresponding surface concentration profiles show, as expected, an enhanced agglomeration of contractile filaments at the equator (figure 6). This combination between aggregation of filaments and their circumferential orientation conforms to the experimental observation that a high concentration of oriented filaments appears under the furrow leading edge only after the induction of surface deformation, and develops simultaneously with cleavage progress (Schroeder

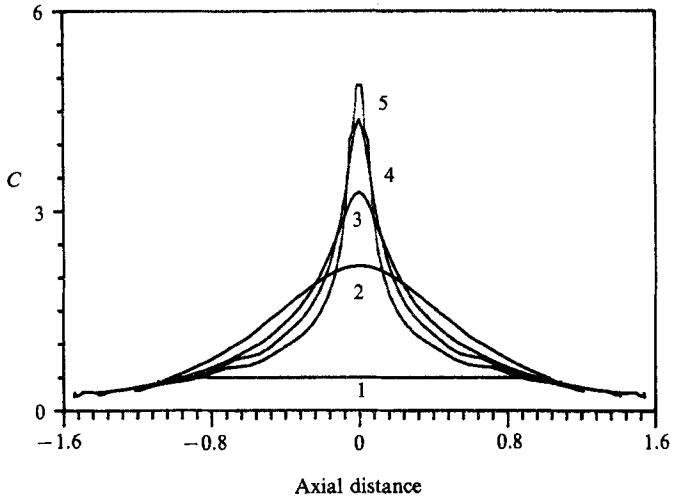

FIGURE 6. Filaments concentration profiles at $t = 0, 2, 3, 4, 5$, respectively.

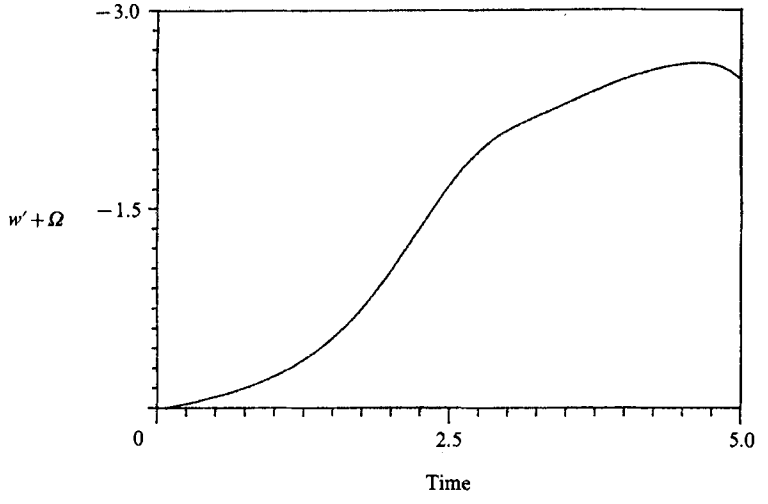

FIGURE 7. The change of rotation intensity in the equatorial region during cleavage. w' and Ω are defined in equation (3.21).

1973, 1987). It may then provide a mechanism for the contractile ring formation. The intensity of rotation which brings about the distinct orientation of the filaments at the equator is depicted in figure 7. It is seen that the rotation coefficient increases to a maximum and then relaxes, the decrease at the least stages of deformation being due to the non-negligible effect of the negatively increasing curvature term in (3.20).

The main factors contributing to the concentration changes are the surface velocity gradients and surface deformations as expressed in the terms on the right-hand side of (3.18). Although initially these two terms contribute to an enhancement of the concentration at the equator, at later stages, when the mean curvature becomes negative, the term that depends on the surface deformation opposes a further increase in concentration. This effect, however, does not become appreciable until the final stages of division and is not perceived in figure 5. It is visible in

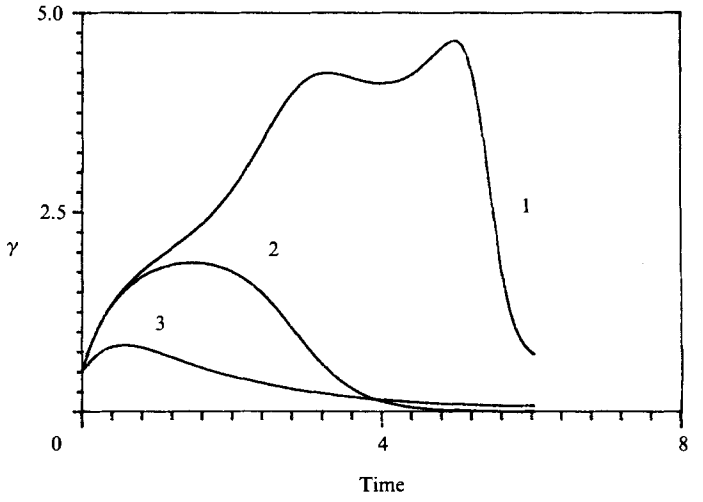

FIGURE 8. Tension dynamics: (1) equatorial circumferential, (2) equatorial meridional, (3) polar.

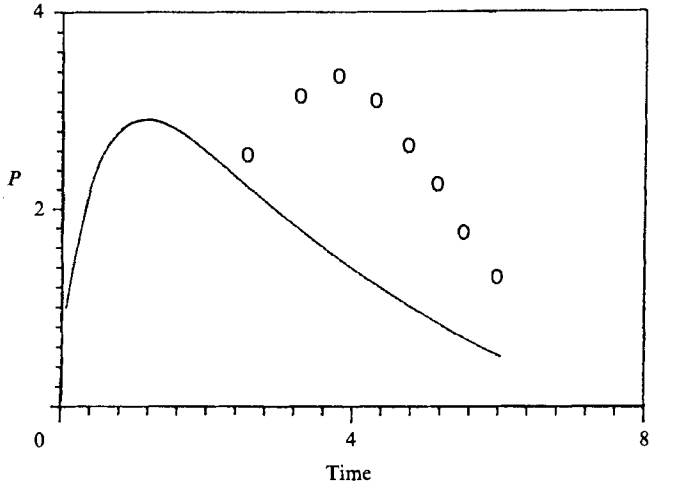

FIGURE 9. Pressure dynamics at the centre O, average estimate by Hiramoto (1968).

figure 7 as mentioned above. The concentration profiles obtained closely resemble the experimental observations on the motion of inert particles on the cell surface during cytokinesis (Rappaport 1978; Koppel, Oliver & Berlin 1982) which show an agglomeration of these particles in the equatorial zone due to surface motions.

A plot of the polar tension and the circumferential and meridional equatorial tensions is presented in figure 8. It is observed that initially all the tensions increase but later diminish. This is due to the combined effect of contractile filament production by the biochemical reaction, muscle dynamics and surface motions. At the onset of the process the increase of tension comes mainly from the reaction and muscle dynamics effects, while deformations and surface motions are still small. The later decrease in the tension is then due to a decrease in the filaments force and the decomposition of active filaments. The effect of surface motion and deformation is more visible in the polar tensions since these rapidly cause a decrease in the polar concentration of active filaments which subsequently lowers the tension there.

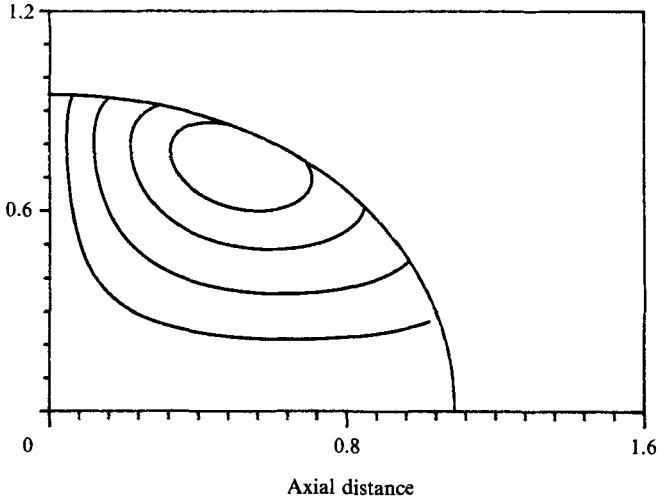

FIGURE 10. Streamline pattern at $t = 2$.

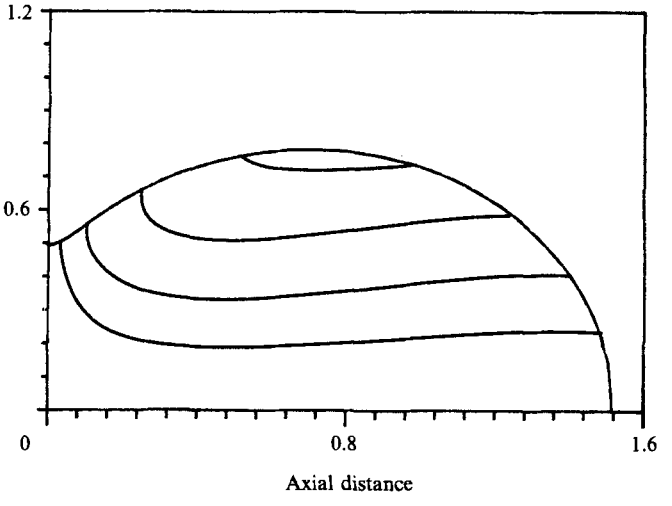

FIGURE 11. Streamline pattern at $t = 4.7$.

Although the general behaviour of these tension agrees with Hiramoto's (1968) observations, his measured values for the polar tension are higher than those of the meridional equatorial component at all times. This discrepancy is a result of the neglected passive surface tension in (2.10). A more complete description of the rheology of the cortical layer is likely to show higher values for the polar tension since major strains occur in that region. This aspect is currently under study. Furthermore, deviations from experimental observation of tension development result also from the simplified form of biochemical scheme and muscle dynamics assumed here. Of course no cleavage will progress without these factors and a better knowledge of these processes still awaits further biochemical research.

Hiramoto (1968) calculated the pressure within the cell from measurements of an external force applied at the polar region. His calculations are compared in figure 9 to the average pressure evaluated by means of (3.17). A qualitatively similar

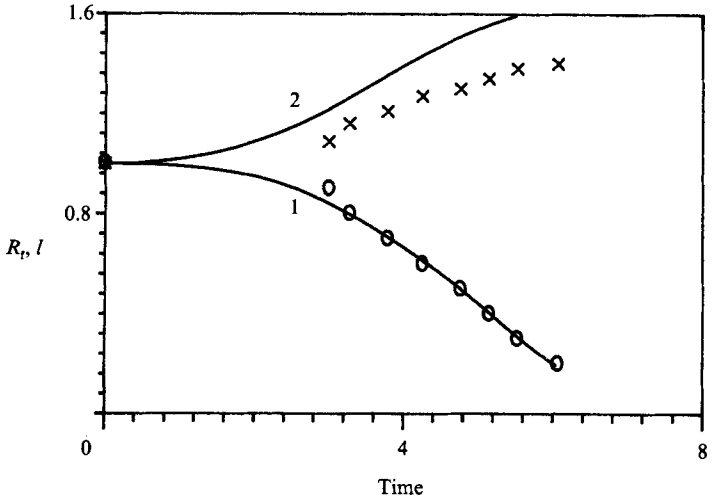

FIGURE 12. Evolution of furrow radius R_f (1) and polar distance l (2) during cytokinesis. Experimental data by Hiramoto (1968).

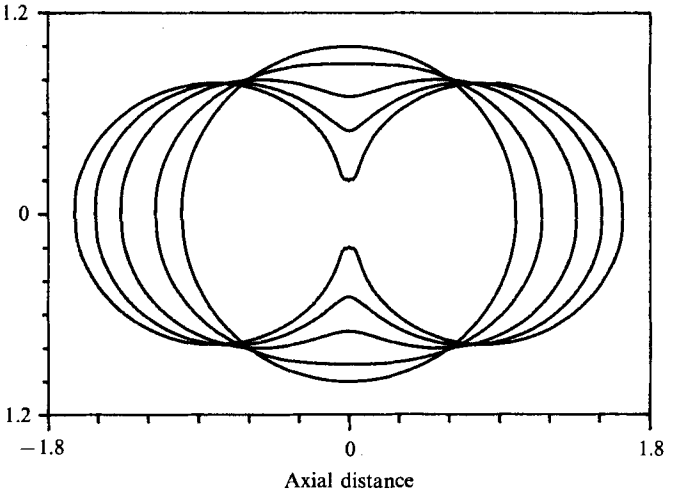

FIGURE 13. Consecutive surface shapes of the dividing cell.

behaviour is observed while the time lag is apparently again due to the simplified biochemical and muscle dynamic schemes assumed and to the arbitrary choice of viscosity ratio in the solution of (2.15). The corresponding streamlines of the cytoplasmic motion calculated at two different times are shown in figures 10 and 11, and exhibit remarkable resemblance to the cytoplasmic motions observed by Hiramoto (1978). Note that the dividing cell surface is not a streamline. Figure 12 depicts the results of the dynamic deformation of the surface during cleavage. The shrinkage of the furrow radius is shown together with the variation in the polar distance and the corresponding experimental observations of Hiramoto (1968). While the dynamics of the furrow radius closely follow that of the experimental findings, the polar distances calculated are slightly higher than those observed. It is anticipated that when more realistic rheological properties for the cortex are incorporated in (2.10), and thereby in (2.15), the discrepancy in the predicted and measured geometrical dimensions will diminish.

In conclusion we emphasize that the realization of a simulation for the complex phenomenon of cell surface deformation to ultimate division is brought about by the employment of a fluid-mechanical analysis combined with biochemical schemes for the development of surface forces. The ultrastructural description of the cortex layer provided an integrated anisotropic surface tension which is otherwise not encountered in pure liquids. The boundary-integral representation for the flow equations facilitated a quasi-steady solution of the moving-boundary problem and a continuous calculation of the corresponding surface deformation. The resulting instantaneous cell shapes, a typical example of which is depicted in figure 13, closely resemble the reported experimental observations (Hiramoto 1968; Karasiewicz 1981).

This research was supported by the Fund for the Promotion of Research at the Technion.

Appendix A. The explicit form of the components of A in (3.11)

$$A_{rr} = -\frac{k}{8\pi}\frac{(1+R'^2(y))^{\frac{1}{2}}}{r^{\frac{3}{2}}R(y)^{\frac{1}{2}}}\left\{[r^2+R^2(y)+2(z-y)^2]F - [2(z-y)^4+3(z-y)^2\,(r^2+R^2(y))+(r^2-R^2(y))^2]\frac{E}{r_{xy}^2}\right\},$$

$$A_{rz} = -\frac{k}{8\pi}\frac{(1+R'^2(y))^{\frac{1}{2}}R^{\frac{1}{2}}(y)}{r^{\frac{3}{2}}}\left\{F+[r^2-R^2(y)-(z-y)^2]\frac{E}{r_{xy}^2}\right\},$$

$$A_{zr} = \frac{k}{8\pi}\frac{(1+R'^2(y))^{\frac{1}{2}}(z-y)}{r^{\frac{1}{2}}R^{\frac{1}{2}}(y)}\left\{F-[r^2-R^2(y)+(z-y)^2]\frac{E}{r_{xy}^2}\right\},$$

$$A_{zz} = -\frac{k}{4\pi}\frac{(1+R'^2(y))^{\frac{1}{2}}R^{\frac{1}{2}}(y)}{r^{\frac{1}{2}}}\left\{F+(z-y)^2\frac{E}{r_{xy}^2}\right\},$$

where $$k^2 = \frac{4rR(y)}{(z-y)^2+[r+R(y)]^2}, \quad r_{xy}^2 = (z-y)^2+[r-R(y)]^2.$$

F and E are the complete elliptical integrals of the first and second kind with modulus k.

Appendix B. The expressions for the components of P in (3.17)

$$P_r = \frac{k}{4\pi}\frac{(1+R'^2(y))^{\frac{1}{2}}}{R^{\frac{1}{2}}(y)\,r^{\frac{1}{2}}}\left\{[R^2(y)-r^2-(y-z)^2]\frac{E}{r_{xy}^2}+F\right\},$$

$$P_z = \frac{k}{2\pi}\frac{(1+R'^2(y))^{\frac{1}{2}}R^{\frac{1}{2}}(y)\,(y-z)}{r^{\frac{1}{2}}}\frac{E}{r_{xy}^2}.$$

REFERENCES

Adin Mann, J. 1984 *Surf. Colloid Sci.* **13**, 145.

Akkas, N. 1980 *J. Biomech.* **13**, 977.

Akkas, N. 1981 *J. Biomech.* **14**, 621.

Aris, R. 1962 *Vector, Tensors and the Basic Equations of Fluid Mechanics.* Prentice-Hall.

Barthes-Biesel, D. 1980 *J. Fluid Mech.* **100**, 831.

Barthes-Biesel, D. & Sgaier, H. 1985 *J. Fluid Mech.* **160**, 119.

Beams, H. W. & Evans, T. C. 1940 *Biol. Bull.* **79**, 188.

Butschli, O. 1876 *Abh. Senckenberg. naturf. Ges., Frankf. M.* **10**, 232.

Conrad, G. W. & Rappaport, R. 1981 In *Mitosis/Cytokinesis* (ed. A. M. Zimmerman & A. Forer), p. 365. Academic.

Cox, R. G. 1969 *J. Fluid Mech.* **37**, 601.

Edidin, N. 1977 *Ann. Rev. Biophys. Bioengng* **3**, 179.

Evans, E. A. & Skalak, R. 1979 *Mechanics and Thermodynamics of Biomembranes.* CRC.

Gallez, D. 1984 *J. Theor. Biol.* **111**, 341.

Geller, A. S., Lee, A. S. & Leal, L. G. 1986 *J. Fluid Mech.* **169**, 27.

Goody, R. S. & Holmes, K. C. 1983 *Biochim Biophys Acta* **726**, 13.

Greenspan, H. P. 1977*a* *J. Theor. Biol.* **65**, 79.

Greenspan, H. P. 1977*b* *Stud. Appl. Maths* **57**, 45.

Greenspan, H. P. 1978 *J. Theor. Biol.* **70**, 135.

Higdon, J. J. L. 1985 *J. Fluid Mech.* **159**, 195.

Hiram, Y. & Nir, A. 1983 *J. Colloid Interface Sci.* **95**, 462.

Hiramoto, Y. 1956 *Expl Cell. Res.* **11**, 630.

Hiramoto, Y. 1968 *22nd Symp. Soc. Expl Biol.*, p. 311.

Hiramoto, Y. 1978 *Dev. Grow. Diff.* **13**, 191.

Karasiewicz, J. 1981 In *Mitosis/Cytokinesis* (ed. A. M. Zimmerman & A. Forer), p. 419. Academic.

Koppel, D. E., Oliver, J. M. & Berlin, R. D. 1982 *J. Cell. Biol.* **93**, 950.

Ladyzhenskaya, D. A. 1969 *The Mathematical Theory of Viscous Incompressible Flow*, 2nd edn. Gordon and Breach.

Lanir, Y. 1983 *J. Biomech.* **16**, 1.

Leal, L. G. & Hinch, E. J. 1971 *J. Fluid Mech.* **46**, 685.

Lee, S. H. & Leal, L. G. 1982 *J. Colloid Interface Sci.* **87**, 81.

Levich, V. G. & Krylov, V. S. 1969 *Ann. Rev. Fluid Mech.* **1**, 293.

Pujara, P. & Lardner, T. J. 1979 *J. Biomech.* **12**, 293.

Rallison, J. M. & Acrivos, A. 1978 *J. Fluid Mech.* **89**, 191.

Rappaport, R. 1978 *J. Exp. Zool.* **206**, 1.

Rappaport, R. & Ebstein, R. P. 1965 *J. Exp. Zool.* **158**, 373.

Sapir, T. 1984 Surface tension driven motion of interfaces. M.Sc. thesis, Technion.

Sapir, T. & Nir, A. 1985 *Physico. Hydrodyn.* **6**, 803.

Schroeder, T. E. 1973 *Proc. Natn. Acad. Sci. USA* **70**, 1688.

Schroeder, T. E. 1975 In *Molecules and Cell Movement* (ed. S. Inoue & E. R. Stephens), p. 305. NY: Raven.

Schroeder, T. E. 1981*a* In *Cytoskeletal Elements and Plasma Membrane Organization* (ed G. Poste & G. K. Nicolson), p. 169. Elsevier.

Schroeder, T. E. 1981*b* *Expl Cell. Res.* **134**, 231.

Schroeder, T. E. 1987 In *The Biomechanics of Cell Division* (ed. N. Akkas), p. 209. Plenum.

Spek, J. 1918 *Arch. f. Entw. Mech.* **44**, 5.

Waxman, A. M. 1981 *J. Non Newtonian Fluid Mech.* **9**, 235.

WAXMAN, A. M. 1984 *Stud. Appl. Maths* **66**, 189.

WHITE, J. G. & BORISY, G. G. 1983 *J. Theor. Biol.* **101**, 289.

YOUNGREN, G. K. & ACRIVOS, A. 1975 *J. Fluid Mech.* **69**, 377.

YOUNGREN, G. K. & ACRIVOS, A. 1976 *J. Fluid Mech.* **76**, 433.

ZINEMANAS, D. & NIR, A. 1987 In *The Biomechanics of Cell Division* (ed. N. Akkas), p. 281. Plenum.